Imaging Microglia and Astrocytes non-invasively using Diffusion MRI

Raquel Garcia-Hernandez [1], Alejandro Trouve Carpena[1], Mark Drakesmith[2], Kristen Koller[2], Derek K. Jones[2], Santiago Canals[1]* and Silvia De Santis[1,2]*

[1]Instituto de Neurociencias, CSIC/UMH, San Juan de Alicante, Alicante, Spain.

[2]CUBRIC, School of Psychology, Cardiff University, Cardiff, UK

Keywords: Neuroinflammation, glial reaction, LPS, PLX5622, Microglia, Astrocytes, diffusion MRI

Abstract

We present a strategy to image neuroinflammation in grey matter using diffusion-weighted MRI. We demonstrate that the MRI signal carries the fingerprint of microglia and astrocytes activation, and that specific signatures from each glia population can be extracted *in vivo*. In addition, we prove the translational value of the approach in a cohort of healthy humans. This framework will aid basic and clinical research to clarify the role of inflammation during lifespan.

Main

Introduction

Neurodegenerative diseases such as Alzheimer's, Parkinson's, multiple sclerosis and dementia are among the most pressing problems of developed societies with aging populations [1-3]. Accumulating evidence suggests chronic neuroinflammation, the sustained activation of microglia and astrocytes in the brain, to strongly influence neurodegeneration and contribute to its progression. In addition, abnormal immune activation during puberty and adolescence has been recognized to increase vulnerabilities to brain disorders later in life [4], making the characterization of the inflammatory profile along the lifespan a hot topic. A major question is whether inhibition of the inflammatory response has the ability to reverse or slow down its symptoms [5]. Therapies targeting glial cells are currently being proposed as disease-altering treatments to improve the outcome of neurological disorders, with extremely promising results [5-7]. Furthermore, for many brain diseases [8], neuroinflammation is emerging as a cause, rather than a consequence of the pathogenesis, thus, characterizing the tissue inflammatory state could serve as valuable early disease biomarkers.

While imaging techniques are widely adopted to monitor neurologic conditions, non-invasive approaches able to specifically characterize brain inflammation *in vivo* are lacking. The current gold-standard is positron emission tomography (PET)-based targeting of the 18kDa translocator protein. While difficult to generalize due to different binding genotypes across individuals [9], PET is associated with ionizing radiation exposure, which limits its use in vulnerable populations and longitudinal studies, and also has low spatial resolution, making it unsuitable to image small brain structures. Diffusion-weighted magnetic resonance imaging (DW-MRI), on the other hand, has the unique ability to image brain microstructure *in vivo*, non-invasively and with high resolution by capturing the random motion of water molecules in brain parenchyma [10].

While the DW-MRI signal is potentially sensitive to all extracellular and intracellular spaces that define water restriction pools in the tissue, current formulations are mostly designed for white matter and axons. However, by combining advanced DW-MRI sequences, the neurobiological knowledge about brain parenchyma, and proper mathematical models, the diffusion characteristics within specific tissue compartments, and even cell types, could be measured.

With this idea in mind, we developed an innovative strategy to image microglia and astrocyte activation in grey matter using DW-MRI, by building a microstructural multi-compartment tissue model based on microglia and astrocyte morphology. To validate the model, we used an established rat paradigm of inflammation based on intracerebral lipopolysaccharide (LPS) administration [11]. In the initial stages of this paradigm, neuronal viability and morphology is preserved, while inducing a

microglia activation within few hours, and delayed astrocytic response detectable only 24 hours after the injection [12]. Therefore, a glial response can be transiently dissociated from neuronal degeneration, and the signature of reactive microglia investigated independently of any astrogliosis. Furthermore, to isolate the imaging fingerprint of astrocytes activation, we repeated the experiment in rats previously treated with the CSF1R-inhibitor PLX5622 (Plexxikon Inc.), which is known to temporally deplete up to 90% of the microglia population [13].

We demonstrate, for the first time, that DW-MRI signal carries the fingerprint of microglia and astrocytes activation, and that signatures specific to each glia population, reflecting the morphological changes as validated *post-mortem* by quantitative immunohistochemistry, can be extracted *in vivo*. In addition, we demonstrate the translational value of the approach in a cohort of healthy humans, in which we performed a reproducibility analysis. A framework able to characterize relevant aspects of tissue microstructure during inflammation *in vivo* and non-invasively, is expected to have a tremendous impact on our understanding of the pathophysiology of many brain conditions, and transform current diagnostic practice and treatment monitor strategies.

Results

We first built a model of grey matter diffusivity to account for water diffusion in a microglial compartment corresponding to small cell somas (modeled as small spheres) and thin cellular processes (modeled as sticks) growing radially from the soma with a certain dispersion, and an astrocytic compartment consisting on large globular cells (modeled as large spheres) [14], both of them embedded in an extracellular space compartment, as detailed in the methods section. We then tested the mathematical model with an experimental paradigm of neuroinflammation, induced by an injection of LPS in one hemisphere (targeting the dentate gyrus of the hippocampus) and with the contralateral side as within-subjects control (vehicle injected, see methods for details).

Morphological analysis of Iba-1^+ cells by histology in the tissue at different time-points after LPS injection demonstrate a fast microglial reaction with retraction of cellular processes at 8h, that progresses at 24 h with an additional increase in the microglial cell body size and a reduction in the processes dispersion, as shown in Fig. 1 b-c. The distinct and time-dependent changes in microglial cell morphology are tightly mirrored by the imaging parameters specifically related to the microglia compartment, i.e., the sticks (cellular processes) and the small spheres (cell soma). Accordingly, the stick fraction is significantly reduced at 8 hours in the injected hippocampus compared to the control side, and further reduced at 24 hours. The radius of the small sphere component is significantly increased at 8 and 24 hours. Importantly, these LPS-induced changes disappear when the animals are depleted of microglia by the pretreatment with PLX5622, demonstrating that the MRI signatures are specific to the microglia population. Moreover, when looking at inter-individual variability, a strong association was found

between MRI-derived microglial markers and their histological counterparts at all measured time points (Fig. 1e-f). Finally, at 2 weeks post-injection, when complete recovery is expected, all parameters measured from both histology and MRI converge, showing no statistically significant difference between injected and control hemisphere. Overall, these results demonstrate the possibility to recover a microglia-specific signal from DW-MRI with capacity to unmask a microglial reaction *in vivo* (Fig. 1g).

We next performed a comparable analysis with astrocytes (labeled as $GFAP^+$ cells) taking advantage of the distinct time course of their response to LPS injection. This cell population, unlike microglia, shows no significant alteration neither in density nor morphology at 8h post LPS injection, as shown in Fig.2b and supplementary Fig 7. However, at 24h, astrocytes grow in volume as measured by the mean radius of the convex hull (Fig. 2, see methods for details). Interestingly, the associated MRI compartment for astrocytes, i.e. the large spheres, follows the same pattern of changes across conditions. Volume of $GFAP^+$ cells and the mean radius of the large spheres measured by DW-MRI grew in parallel at 24h post LPS injection, were insensitive to microglia depletion with PLX5622 pretreatment and recovered towards baseline levels at 15 days post-injection. Accordingly, their inter-individual variability showed a strong correlation (Fig. 2d). Therefore, the results obtained for the astrocytic component also demonstrate the possibility to recover an astrocyte-specific signal from DW-MRI with capacity to map an astrocyte reaction *in vivo* (Fig. 1g).

To highlight the importance of the developed framework, it is important to show that conventional MRI is sensitive to morphological changes due to inflammation, but cannot disentangle the different populations involved across different conditions, as shown in Fig. S4. An increase in mean diffusivity reflects mostly changes in the extra-cellular space. A clear reduction of T1/T2 is observed in all three conditions, while no myelin change is observed in histology (Fig. S3). T2* does not have enough sensitivity to reflect glia morphological changes at any stages.

As a proof of concept for the translational validity of these results and to evaluate the reproducibility of the proposed imaging framework, we adapted the MRI protocol to a human 3T Connectom scanner [15] and acquired data from a healthy cohort. As shown in Fig. 3, the multi-compartment model applied to these data returned values for the coefficient of variations (CoV) within-subjects in the range 1.5-8%, and CoV between-subjects in the range 2.6-15, which is in the range of conventional MRI measures routinely used in the clinics with diagnostic value. Finally, we took advantage of the known heterogeneous distribution of microglial cell densities across brain regions in humans to test the ability of our framework to quantify microglial cell populations *in vivo*. Importantly, we found that the stick fraction calculated across different grey matter regions follows the patterns of microglia cell density measured *post mortem* in humans [16], with the hippocampus showing the largest volume fraction (Fig. S5).

Discussion

Diffusion MRI signal has great potential to reveal the inflammatory component in numerous brain conditions [17], and several efforts have been made to provide microstructural models able to capture features belonging to distinct tissue sub-compartments, for example by including dendrites dispersion [18, 19] or a compartment for the soma of neurons [20]. However, so far, no framework was available to specifically look at the cellular signature of glia activation. Here we propose and validate a strategy to image microglia and astrocyte activation in grey matter using diffusion MRI, and demonstrate its translational validity to humans. By taking advantage of the different activation windows of glia in an LPS-driven immunological challenge in rats, and by using pharmacological tools to deplete microglia in the brain, we were able to dissect the MRI signatures of specific glial responses. We identified two MRI parameters, namely the stick fraction and the larger sphere size, as sensitive to, and only to, microglia and astrocyte activation, respectively.

Our results are supported by quantitative cell morphology analysis. Validation of MRI results is challenging due to several factors, including the need to co-register regions of interest with very different sizes and properties and the need for tissue fixation in the histological preparations [21]. To overcome this limitation, here we relied on measuring changes rather than absolute magnitude of quantities. We demonstrate that there is a very high correlation between the changes found in injected *vs*. control regions, as measured using MRI and histology, suggesting that our imaging measures truly capture the hallmark of glia activation with high sensitivity.

The proposed MRI methodology was adapted to a human MRI scanner, and healthy subjects were recruited to perform a reproducibility study, demonstrating that the glia biomarkers are highly reproducible between different MRI sessions and in line with CoVs calculated for conventional MRI parameters routinely used in clinical settings [22].

Our results have implications in the interpretation of several imaging studies published so far. We propose that since diffusion MRI signal is sensitive to glia activation, the biological substrate of some of the alterations reported in numerous brain conditions could be driven by changes in glia morphology, rather than the conventional interpretation as “neural damage or degeneration”. For example, multiple sclerosis (MS) is known to have a strong inflammatory component [2] and while DW-MRI is widely applied to characterize brain damage in MS, current approaches cannot differentiate between glia activation and neuronal damage.

This study has some limitations. While the multicompartment model does not explicitly differentiate between microglia processes and dendrites, basic geometrical reasoning supports the idea that neuronal loss would increase the stick dispersion, rather than decreasing it, and would thus be easily distinguished from a microglia activation, although this claim needs to be proven in future studies.

To conclude, we proposed here a new generation of non-invasive glia-centric biomarkers, which are expected to transform the study of many diseases associated with a glial response: those where inflammation is as a known or possible cause, as well as those in which the glial reaction can serve as a powerful early diagnostic and/or prognostic marker.

Figures

Fig. 1: Histological characterization of microglia reaction and its associated MR imaging signature.

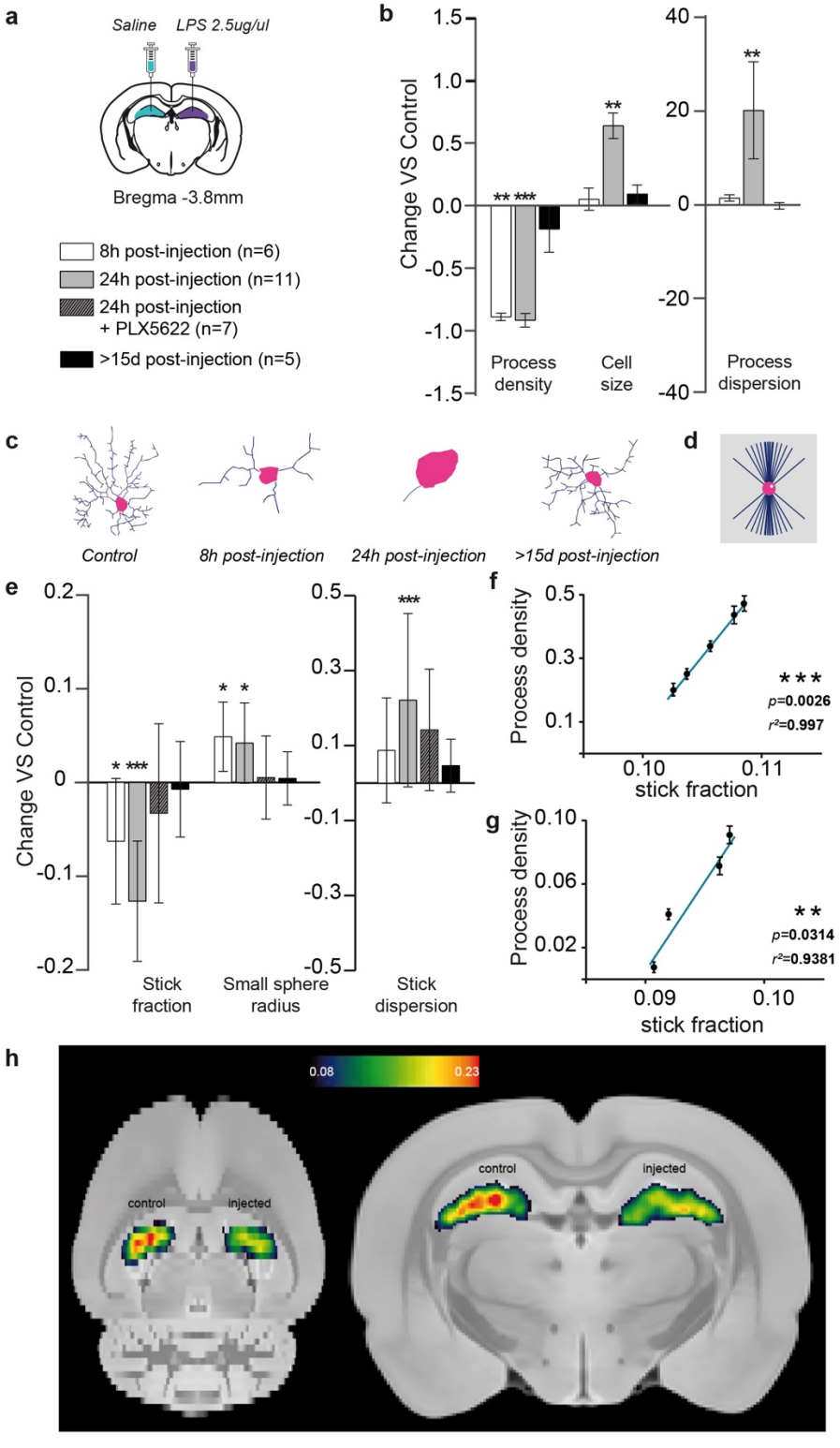

a, experimental scheme showing bilateral stereotaxic injection of LPS (left) / saline (right) and the composition of the four groups: 6 animals were scanned 8 hours post-injection, 11 animals were scanned 24 hours post-injection, 8 animals were treated with PLX5622 for 7 days before the injection and then scanned 24 hours post-injection, and 5 animals were scanned 15 days or more post-injection. **b**, normalized change $(P_{injected}-P_{control})/P_{control}$ in process density, cell size and process dispersion for the injected versus control hippocampus, measured in Iba-1^{+} stained microglia for the different groups.

Asterisks represent significant paired difference between injected and control. **c**, morphology reconstruction of representative microglia at the different times. **d**, geometrical model used for microglia. **e**, normalized change $(P_{injected}-P_{control})/P_{control}$ between MRI parameter calculated in the injected vs control hemisphere for the microglia compartment. Asterisks represent significant paired difference between injected and control. **f**, **g**, correlations between stick fraction from MRI and process dispersion from Iba-1 at 8 (e) and 24 hours post injection (f). **h**, mean stick fraction maps at 24 h post-injection, normalized to a rat brain template and averaged over all rats.

Fig. 2: Histological characterization of astrocyte reaction and its associated MR imaging signature.

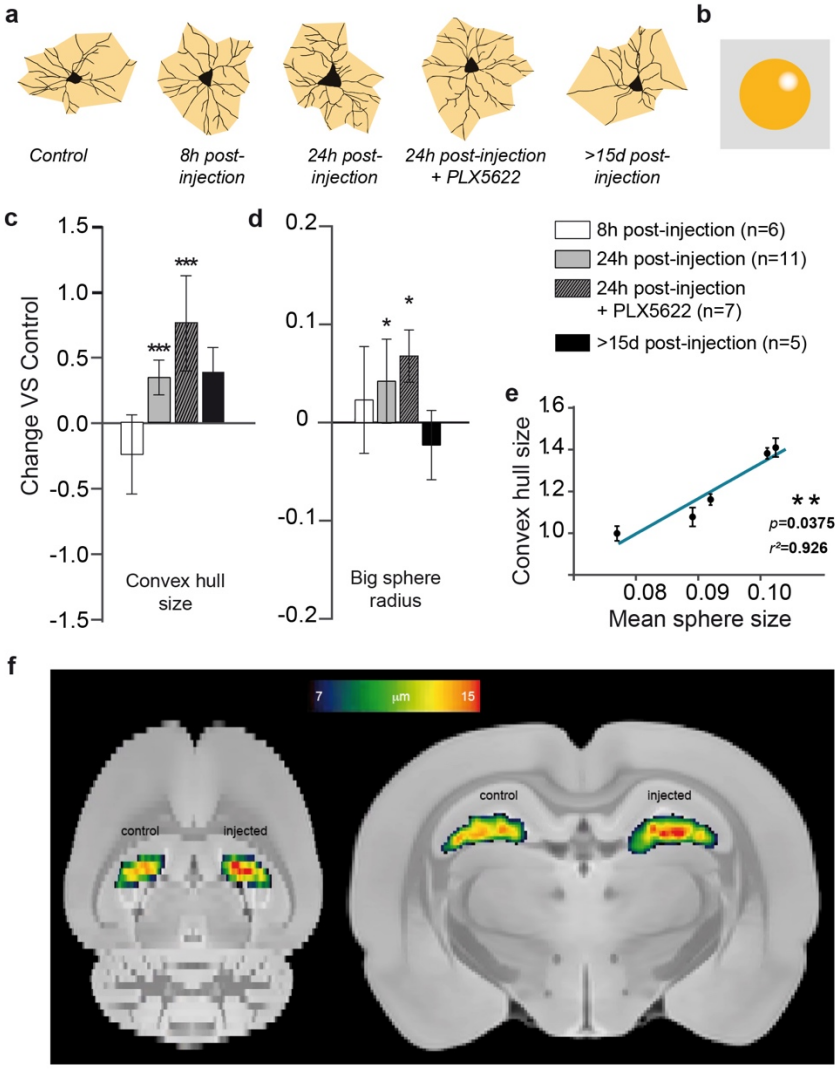

a, morphology reconstruction of representative astrocytes at the different times in black and 2-D convex hull in grey. **b**, geometrical model used for astrocites. **c**, normalized change $(P_{injected}-P_{control})/P_{control}$ in convex hull mean radius for the injected versus control hippocampus, measured in $GFAP^{+}$ stained astrocytes for the different groups. Asterisks represent significant paired difference

between injected and control. **d**, normalized change $(P_{injected}-P_{control})/P_{control}$ between MRI-derived large sphere radius calculated in the injected vs control hemisphere for the astrocyte compartment (shown in the insert). Asterisks represent significant paired difference between injected and control. **e**, correlation between mean sphere radius from MRI and convex hull mean radius from GFAP. **e**, large sphere radius maps at 24 h post-injection, normalized to a rat brain template and averaged over all rats.

Fig. 3: Feasibility of the framework translation to humans and MR parameters reproducibility analysis

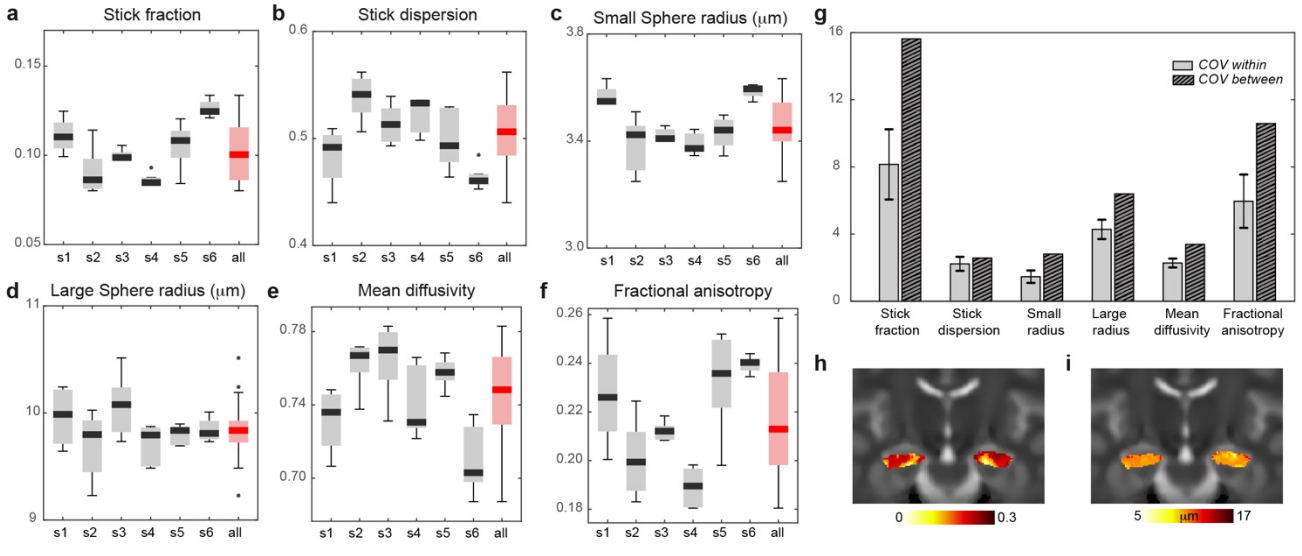

a, boxplot of stick fraction as measured separately in the hippocampus of 6 subjects scanned 5 times (s1-s6) and pooling all subject together (red). The same is shown for the stick dispersion (**b**), small (**c**), large sphere radius (**d**), mean diffusivity (**e**) and fractional anisotropy (**f**). **g**, average coefficient of variation calculated within subject (light grey) and between subjects (striped). **h**, mean stick fraction map in the hippocampus averaged in the whole cohort. **i**, mean large sphere radius map in the hippocampus averaged in the whole cohort.

Acknowledgements

We thank Thomas Witzel for his help with the pulse sequence, Jose Lopez-Atalaya for advising on microglia activation and manipulation techniques and Begoña Fernandez for excellent technical assistance. We thank Plexxikon Inc. (USA) for providing PLX5622 chow and for technical advice. SdS was supported by the European Research Council through a Marie Skłodowska-Curie Individual Fellowship (Grant #749506) and by the Generalitat Valenciana through a Subvencion a la Excelencia de

Juniors Investigadores (SEJI/2019/038). SC was supported by the Spanish Agency of Research (AEI) under the grant PGC2018-101055-B-I00, co-financed by the European Regional Development Fund (ERDF), the Generalitat Valenciana through the program Prometeo/2019/015, and the European Union Horizon 2020 research and innovation program under Grant 668863 (SyBil-AA). SdS and SC also acknowledge financial support from the Spanish State Research Agency through the Severo Ochoa Program for Centres of Excellence in R&D (SEV- 2017-0723). The human data were acquired at the UK *National Facility for In Vivo MR Imaging of Human Tissue Microstructure* funded by the EPSRC (grant EP/M029778/1), and The Wolfson Foundation. DKJ is supported by a Wellcome Trust Investigator Award (096646/Z/11/Z) and a Wellcome Trust Strategic Award (104943/Z/14/Z).

Bibliography

1. Ransohoff, R. M. How neuroinflammation contributes to neurodegeneration. *Science* **353**, 777-83 (2016).

2. Lassmann, H., van Horssen, J. & Mahad, D. Progressive multiple sclerosis: pathology and pathogenesis. *Nat Rev Neurol* **8**, 647-56 (2012).

3. Glass, C. K., Saijo, K., Winner, B., Marchetto, M. C., & Gage, F. H. Mechanisms Underlying Inflammation in Neurodegeneration. *Cell* **140**, 918-934 (2010).

4. Yahfoufi, N., Matar, C. & Ismail, N. Adolescence and aging: impact of adolescence inflammatory stress and microbiota alterations on brain development, aging and neurodegeneration. *J Gerontol A Biol Sci Med Sci.* doi: 10.1093/gerona/glaa006 (2020).

5. Janus, C., Pearson, J., McLaurin, J., Mathews, P.M., Jiang, Y., Schmidt, S.D., Chishti, M.A., Horne, P., Heslin, D. & French, J. Aβ peptide immunization reduces behavioural impairment and plaques in a model of Alzheimer's disease. *Nature* **408**, 979–982 (2000).

6. Wilbanks, B., Maher, L.J. 3rd & Rodriguez, M. Glial cells as therapeutic targets in progressive multiple sclerosis. *Expert Rev Neurother* **19** 481-494 (2019).

7. Samis Zella, M. A., Metzdorf, J., Ostendorf, F., Maass, F., Muhlack, S., Gold, R., Haghikia, A. & Tönges, L. Novel Immunotherapeutic Approaches to Target Alpha-Synuclein and Related Neuroinflammation in Parkinson's Disease. *Cells* **8**, 105 (2019).

8. Amor, S., Puentes, F., Baker, D. & van der Valk, P. Inflammation in neurodegenerative diseases. *Immunology* **129**, 154–169 (2010).

9. Owen, D. R., Gunn, R. N., Rabiner, E. A., Bennacef, I., Fujita, M., Kreisl, W. C., Innis, R. B., Pike, V. W., Reynolds, R., Matthews, P. M. & Parker, C. A. Mixed-affinity binding in humans with 18-kDa translocator protein ligands. *J Nucl Med* **52**, 24-32 (2011)

10. Pierpaoli, C. & Basser, P. J. Toward a quantitative assessment of diffusion anisotropy. *Magn Res Med* **36**, 893 (1996)

11. Espinosa-Oliva, A. M., de Pablos, R. M. & Herrera, A. J. Intracranial injection of LPS in rat as animal model of neuroinflammation. *Methods Mol Biol* **1041**, 295-305 (2013).

12. Jeong, H. K., Jou, I. & Joe, E. H. Systemic LPS administration induces brain inflammation but not dopaminergic neuronal death in the substantia nigra. *Exp Mol Med*. **42**, 823-32 (2010).

13. Han, J., Harris, R. A. & Zhang, X-M. An updated assessment of microglia depletion: current concepts and future directions. *Mol Brain* **10**, 25 (2017).

14. Verkhratsky, A. & Butt A. Morphology of Glial Cells. In Glial Neurobiology: a textbook, John Wiley and sons (2007).

15. Jones, D. K., Alexander, D. C., Bowtell, R., Cercignani, M., Dell'Acqua, F., McHugh, D. J., Miller, K. L., Palombo, M., Parker, G. J. M., Rudrapatna, U. S. & Tax, C. M. W. Microstructural imaging of the human brain with a 'super-scanner': 10 key advantages of ultra-strong gradients for diffusion MRI. *Neuroimage* **182**, 8-38 (2018).

16. Mittelbronn, M., Dietz, K., Schluesener, H. J. & Meyermann, R. Local distribution of microglia in the normal adult human central nervous system differs by up to one order of magnitude. *Acta Neuropathol* **101**, 249-55 (2001).

17. De Santis, S., Canals, S. Non-invasive MRI windows to neuroinflammation. *Neuroscience* **403**, 1-3 (2019).

18. Jespersen, S. N., Kroenke, C. D., Østergaard, L., Ackerman, J. J. & Yablonskiy, D. A. *Neuroimage* **34**, 1473 (2007).

19. Zhang, H., Schneider, T., Wheeler-Kingshott, C. A. & Alexander, D. C. *Neuroimage* **61**, 1000 (2012).

20. Palombo, M., Ianus, A., Nunes, D., Guerreri, M., Alexander, D. C., Shemesh, N. & Zhang, H. SANDI: a compartment-based model for non-invasive apparent soma and neurite imaging by diffusion MRI. arXiv:1907.02832.

21. Horowitz, A., Barazany, D., Tavor, I., Yovel, G. & Assaf, Y. *Brain Struct Funct* **220**, 1791-1792 (2015).

22. Veenith, T. V., Carter, E., Grossac, J., Newcombe, V. F., Outtrim, J. G., Lupson, V., Williams, G. B., Menon, D. K. & Coles, J. P. Inter subject variability and reproducibility of diffusion tensor imaging within and between different imaging sessions. *PLoS One* **8**, e65941 (2013)

Online Methods

Animal preparation

All animal experiments were approved by the Animal Care and Use Committee of the Instituto de Neurociencias de Alicante, Alicante, Spain, and comply with the Spanish (law 32/2007) and European regulations (EU directive 86/609, EU decree 2001-486, and EU recommendation 2007/526/EC). Rats were housed in groups (4-5), with 12-12h light/dark cycle, lights on at 8:00, at room temperature (23 ± 2ºC) and free access to food and water. Microglia activation was achieved by intracranial injection in the dorsal hippocampus (coordinates bregma -3.8 mm, sup-inf 3.0 mm, 2 mm from midline in the left hemisphere) of 2 µl of saline and LPS at concentration of 2.5 µg/µl. The opposite hemisphere was injected with the same amount of saline. In a cohort of animals, microglia depletion was achieved by administering the CSF1R-inhibitor PLX5622 (Plexxikon Inc.) in two ways: as a dietary supplement in standard chow at 1200 ppm (Research Diets), and with intraperitoneal injection of 50 mg/kg in vehicle once a day for 7 days. Another cohort of rats received the same chow without enrichment, and was injected IP once a day with the same doses of vehicle. Less than 24 hours after the last injection, all the rats were injected LPS according to the procedure described above.

After different post-injection delays, the rats were scanned in a Bruker 7T MRI scanner using a diffusion-weighted sequence and immediately perfused for *ex-vivo* MRI immunohistological analysis of microglia (Iba-1+) and astrocytes (GFAP+). A total of 27 rats were used, with weights in the range 250gr-300gr, divided in 5 groups. Group 1 (n=6) received the LPS injection, and was scanned and perfused after 8 hours. Group 2a (n=7) received the LPS injection and was scanned and perfused after 24 hours. Group 2b (n=4) was treated with control chow and injected with vehicle for 7 days, then received the LPS injection and was scanned and perfused after 24 hours. Group 3 (n=6) was treated with PLX5622 for 7 days, then received the LPS injection and was scanned and perfused after 24 hours. Group 4 (n=6) received the LPS injection and was scanned and perfused after a minimum of 15 days, or more if the ventricular enlargement was not reabsorbed. No statistically significant differences were detected between group 2a and b (control for PLX5622 chow), so they were merged into a single group for the rest of the analysis. Experimental design is reported in Fig. S1.

MRI experiment

Rats

MRI experiments on rats were performed on a 7 T scanner (Bruker, BioSpect 70/30, Ettlingen, Germany) using a receive-only phase array coil with integrated combiner and preamplifier in combination with an actively detuned transmit-only resonator. DW-MRI data were acquired using an

EchoPlanar Imaging diffusion sequence, with 30 uniform distributed gradient directions, b = 2000 and 4000 s/mm2, diffusion times 15, 25, 40 and 60 ms with four non-diffusion weighted images, repetition time (TR) = 7000 ms and echo time (TE) = 25 ms. Fourteen horizontal slices were set up centered in the hippocampus with field of view (FOV) = 25 × 25 mm^2, matrix size = 110 × 110, in-plane resolution = 0.225 × 0.225 mm^2 and slice thickness = 0.6 mm. Additionally, three relaxometry sequences were acquired with the same geometry of the DW-MRI scan: a gradient echo sequence with TR = 1500 ms, 30 TE equally spaced between 3.3 and 83.4 ms and 3 averages; a T1-weighted sequence with TR = 300 ms. TE = 12.6 ms and 2 averages; and a T1-weighted sequence with TR = 3000 ms. TE = 7.7 ms and 4 averages. Finally, a high-resolution anatomical scan with full brain coverage was acquired with TR = 8000 ms. TE = 14 ms, 4 averages, FOV = 25 × 25 mm^2, matrix size = 200 × 200, in-plane resolution = 0.125 × 0.125 mm^2, 56 slices of thickness = 0.5 mm. Total scan time including animal positioning was around 2 hours.

Humans

6 healthy subjects were scanned 5 times in a 3T Siemens Connectom scanner. DW-MRI data were acquired using an EchoPlanar Imaging diffusion sequence, TE=80 ms, TR 3.9 s, diffusion times 17.3, 30, 42 and 55 ms, bvalues 2000 and 4000 s/mm2, each with 30 and 60 uniformly orientated gradient directions, respectively, and 6 unweighted (b=0) images per diffusion time, yielding a total 384 images. flip angle 90, slice thickness, 2mm, in-plane voxel size: 2mm, FoV: 220x220 mm, Matrix size: 110x110.

MRI analysis and statistics

Rat MRI data were processed as follows. Preliminary data were used to verify the reach of a 2µl injection, confirming that the liquid diffused up to 2.6 mm. So, regions of interest (ROIs) for the analysis were manually drawn in the dentate gyrus of the dorsal hippocampus; the injection tract was used to locate the central slice, and ROIs were drawn from two slices before the injection, and up to 2 slices after, for a total length of 3 mm covered.

Raw DW-MRI data were non-linearly registered to the T2-weighted scan to correct for EPI distortions, corrected for motion and eddy current distortions using affine registration, then fed to a custom routine written in Matlab (R2018a, the Mathworks) which fits the signal to a multi-compartment model (MCM) of diffusion The MCM is inspired by the AxCaliber model for white matter [23] but is adapted to grey matter morphology. The model comprises: one compartment of water undergoing restricted diffusion in cylindric geometry (representing water trapped into cell ramifications) with a main orientation and a Watson dispersion term [24], two spherically restricted compartments [25], and one

extracellular space matrix, aligned with the main cylinder orientation and modelled as a tensor. The fitting parameters are the fraction of water undergoing restricted diffusion in cylinders, the two fraction of water undergoing restricted diffusion in the two spherical compartments, the radii of the two spherical compartments (a smaller and a larger one), and the extra-cellular tensor diffusivity. The MCM is illustrated in Fig. S2. The low b-value shell was used to fit the conventional tensor model and produce maps of the mean diffusivity. T1 and T2 weighted maps were also used to calculate the T1/T2 ratio, which is considered a proxy for myelination [26]. T2* maps were calculating by fitting an exponential decay to the T2*-weighted images acquired at different echo times. Additionally, for illustration purposes the high-resolution anatomical scans were non-linearly registered to a rat brain template [27] using an advanced normalization approach [28]. Repeated measure ANOVA was used to check for significant effect of the injection and of the group.

Similarly, human MRI data were preprocessed as follows. Motion, eddy current and EPI distortions were corrected using FSL TOPUP and EDDY tools [29]. Correction for gradient non-linearities [30-31], signal drift [32] and Gibbs ringing artefacts [33] was also performed. All diffusion data were then registered to a skull-stripped [34] structural T1-weighted image using EPIREG [27].
B0 scans were non-linearly registered to a high-resolution human brain template [35] using an advanced normalization approach [28]; then, the inverse transformation was applied to bring the Desikan GM parcellation in the single subject space. Mean values of all MRI parameters were calculated by averaging the maps in the left and right hippocampi. Both intra and inter-subject coefficient of variations were calculated for each MRI measure.

Tissue processing and immunohistochemistry

Rats were deeply anesthetized with a lethal dose of sodium pentobarbital, 46mg/kg, injected intraperitoneally (Dolethal, E.V.S.A. laboratories., Madrid, España). After, rats were perfused intracardially with 100ml of 0.9% phosphate saline buffer (PBS) and 100ml of ice-cold 4% paraformaldehyde (PFA, BDH, Prolabo, VWR International, Lovaina, Belgium). Then, brains were immediately extracted from the skull and fixed for 1 hour in 4% parafaformaldehyde. Afterwards, brains were included in 3% Agarose/PBS (Sigma-Aldrich, Madrid, Spain), and cut in vibratome (VT 1000S, Leica, Wetzlar, Germany) in 50 µm thick serial coronal sections.

Coronal sections were rinsed and permeabilized three times in 1xPBS with Triton X-100 at 0.5% (Sigma-Aldrich, Madrid, Spain), 10 minutes each one. Then, they were blocked in the same solution with 4% of bovine serum albumin (Sigma-Aldrich, Madrid, Spain) and 2% of goat serum donor herd (Sigma-Aldrich, Madrid, Spain) for 2 hours at room temperature. The slices were then incubated for one night at 4ºC with primary antibodies for Iba-1 (1:1000, Wako Chemicals, Osaka, Japan), GFAP (1:1000, Sigma-

Aldrich, Madrid, Spain) and neurofilament 360Kd medium (1:250, Abcam, Cambridge, United Kingdom) to label microglia, astrocytes and neuron processes respectively. The sections were subsequently incubated in specific secondary antibodies conjugated to the fluorescent probes, each at 1:500 (ThermoFisher Scientific, Waltham, USA) for 2h at room temperature.

Sections were then treated with 4′,6-Diamidine-2′-phenylindole dihydrochloride at 15mM (DAPI, Sigma-Aldrich, Madrid, Spain) during 15 minutes at room temperature, as a tissue contrast. Finally, sections were mounted on slides and covered with an anti-fading medium using a mix solution 1:10 Propyl-gallate:Mowiol (P3130, SIGMA-Aldrich, Madrid, Spain; 475904, MERCK-Millipore, Massachussets, United States).

For myelin labelling, antigen retrieval was performed in 1% citrate buffer (Sigma-Aldrich, Madrid, Spain) and 0.05% of Tween 20 (Sigma-Aldrich, Madrid, Spain) warmed to 80º for protein unmasking. Rest of steps were done as described above, using myelin basic protein primary antibody (MERCK-Millipore, Massachussets, United States).

Imaging and data extraction

The tissue sections were then examined using a computer-assisted morphometry system consisting of a Leica DM4000 fluoresce microscope equipped with a QICAM Qimaging camera 22577 (Biocompare, San Francisco, USA) and Neurolucida morphometric software (MBF, Biosciences, VT, USA). Microglia were visualized and reconstructed under Leica HC PLC APO objective 20x/0.5 and astrocytes under Leica HC PLC APO objective 40x/0.75. Five cells per hippocampus per hemisphere were randomly selected for a total of 540 cells included for analysis (270 microglia, 270 astrocytes). Only cells that displayed intact and clear processes were included. Cells were traced through the entire thickness of the sections, and trace information was then saved as 3D reconstructions or rendered into a 2-dimensional diagram of each cells following analysis requirement.

Metric analysis of reconstructed cells was extracted thanks to Neurolucida Explorer software (MBF, Biosciences, VT, USA) and Imaris (Bitplane, Belfast, United Kingdom): cell body perimeter, number of primary processes, number of nodes (branch points), complexity ([Sum of the terminal orders + Number of terminals] * [Total dendritic length / Number of primary dendrites]), fibres density and dendograms, cell size and polar plots (Fig. S6). Polar plots were analyzed in order to extract fiber orientation and dispersion in a plane parallel to the microscope, where lower values mean an uniform distribution of the fibers around cell body and higher values the opposite. Importantly, 3D convex analysis was performed to estimate astrocytes volume to overcome the limitations of GFAP labelling [36-38]. The volume estimation in analysis is determined from the polygon created from straight lines connecting the most distal points of the astrocytes processes.

Density analysis was performed on 12-bit grey scale pictures acquired with the described system. ROIs were manually delineated following the Franklin and Paxinos rat brain atlas [27], covering the complete hippocampus in each hemisphere, for at least 5 slices per rat. Analysis was performed using Icy software [39] in a semi-automatic manner. The threshold for detection of positive nuclei was set for each condition, setting average nuclei size and a signal/noise ratio higher than 23%, according to Rayleigh criterion for resolution and discrimination between two points.

Myelin and neurofilament fluorescent analysis was also performed on acquired pictures with the described system and analyzed using Icy Software [39]. Two ROIs of 200 μm^2 were placed per hippocampus per hemisphere in at least 5 slices per rat to obtains the corresponding grey values.

Data analysis and statistics

The statistical analysis was done using GraphPad Prism 7 software (GraphPad Software Inc., La Jolla, CA, USA) and Rstudio (RStudio 2015. Inc., Boston, MA). The presence of outlier values and parametric distribution was checked. In most of the analysis we applied t-test comparing, for each time point, control hemisphere versus injected hemisphere. For regression analysis, Pearson's correlation was applied and coefficients were transformed to apply Fisher's 1925 test [40] for significant values. Polar analysis and dispersion estimation was performed to obtain kappa values, before transforming them into an Orientation Dispersion Index (ODI) [41].

Methods references

23. Barazany, D., Basser, P. J. & Assaf Y. In vivo measurement of axon diameter distribution in the corpus callosum of rat brain. *Brain* **132**, 1210-20 (2009).

24. Zhang, H., Schneider, T., Wheeler-Kingshott, C. A. & Alexander, D. C. *Neuroimage* **61**, 1000 (2012).

25. van Gelderen, P., DesPres, D., van Zijl, P. C. & Moonen, C. T. Evaluation of restricted diffusion in cylinders. Phosphocreatine in rabbit leg muscle. *J Magn Reson B* **103**, 255-60 (1994).

26. Glasser, M. F. & Van Essen, D. C. Mapping human cortical areas in vivo based on myelin content as revealed by T1- and T2-weighted MRI. *J Neurosci*. **31**, 11597-616 (2011).

27. Paxinos, G. & Watson, C. The rat brain in stereotaxic coordinates. Elsevier/Academic Press (2009).

28. Klein, A., Andersson, J., Ardekani, B. A., Ashburner, J., Avants, B., Chiang, M. C., Christensen, G. E., Collins, D. L., Gee, J., Hellier, P., Song, J. H., Jenkinson, M., Lepage, C., Rueckert,

D., Thompson, P., Vercauteren, T., Woods, R. P., Mann, J. J. & Parsey, R. V. Evaluation of 14 nonlinear deformation algorithms applied to human brain MRI registration. *Neuroimage* **46**, 786-802 (2009).

29. Andersson, J. L. R. & Sotiropoulos, S. N. An integrated approach to correction for off-resonance effects and subject movement in diffusion MR imaging. *Neuroimage* **125**, 1063-1078 (2016).

30. Glasser, M. F., Sotiropoulos, S. N., Wilson, J. A., Coalson, T. S., Fischl, B., Andersson, J. L., Xu, J., Jbabdi, S., Webster, M., Polimeni, J. R., Van Essen, D. C., Jenkinson, M., & for the WU-Minn HCP Consortium. The Minimal Preprocessing Pipelines for the Human Connectome Project. *Neuroimage* **80**, 105–124 (2013).

31. Rudrapatna, S.U., Parker, G.D., Roberts, J. & Jones D.K. Can we correct for interactions between subject motion and gradient-nonlinearity in diffusion MRI? *Proc. Int. Soc. Mag. Reson. Med.* 1206 (2018).

32. Vos, S. B., Tax, C. M., Luijten, P. R., Ourselin, S., Leemans, A. & Froeling, M. The importance of correcting for signal drift in diffusion MRI. *Magn Reson Med* **77**, 285-299 (2017).

33. Kellner, E., Dhital, B., Kiselev, V. G. & Reisert, M. Gibbs-ringing artifact removal based on local subvoxel-shifts. *Magn Reson Med*. **76**, 1574-1581 (2016).

34. Smith, S. Fast Robust Automated Brain Extraction. *Human Brain Mapping* **17**, 143–155 (2002)

35. Desikan, R. S., Ségonne, F., Fischl, B., Quinn, B. T., Dickerson, B. C., Blacker, D., Buckner, R. L., Dale, A. M., Maguire, R. P., Hyman, B. T., Albert, M. S. & Killiany, R. J. An automated labeling system for subdividing the human cerebral cortex on MRI scans into gyral based regions of interest. Neuroimage **31**, 968-80 (2006).

36. Sofroniew, M. V. & Vinters, H. V. Astrocytes: biology and pathology. *Acta Neuropathol* **119**, 7–35 (2010).

37. Haseleu, J., Anlauf, E., Blaess, S., Endl, E., Derouiche, A. Studying subcellular detail in fixed astrocytes: dissociation of morphologically intact glial cells (DIMIGs). *Front Cell Neurosci* **7**, 54 (2013).

38. Kulkarni, P. M., Barton, E., Savelonas, M., Padmanabhan, R., Lu, Y., Trett, K., Shain, W., Leasure, J. L. & Roysam B. Quantitative 3-D analysis of GFAP labeled astrocytes from fluorescence confocal images. *J Neurosci Methods* **246**, 38–51 (2015).

39. de Chaumont, F., Dallongeville, S., Chenouard, N., Hervé, N., Pop, S., Provoost, T., Meas-Yedid, V., Pankajakshan, P., Lecomte, T., Le Montagner, Y., Lagache, T., Dufour, A. & Olivo-Marin, J.

C. Icy: an open bioimage informatics platform for extended reproducible research. *Nat Methods* **9**, 690–696 (2012).

40. Fisher, R.A. Statistical methods for research Workers. Edinburgh, Scotland: Oliver and Boyd Eds. (1925).

40. Mollink, J., Kleinnijenhuis, M., Cappellen van Walsum, A. V., Sotiropoulos, S. N., Cottaar, M., Mirfin, C., Heinrich, M. P., Jenkinson, M., Pallebage-Gamarallage, M., Ansorge, O., Jbabdi, S. &

Miller, K. L. Evaluating fibre orientation dispersion in white matter: Comparison of diffusion MRI, histology and polarized light imaging. *Neuroimage* **157**, 561–574 (2017).